Accepted for presentation in: the 23rd Conference on the Computation of Electromagnetic Fields COMPUMAG 2021, Cancun, Mexico, January 2022

Model Order Reduction for Thermal Analysis of Wireless Power Transfer Systems Considering Radiation

Myrel Tiemann[1], Markus Clemens[2], and Benedikt Schmuelling[1]
[1]Chair of Electric Mobility and Energy Storage Systems, University of Wuppertal, Wuppertal, Germany
[2]Chair of Electromagnetic Theory, University of Wuppertal, Wuppertal, Germany

This work provides a comprehensive analysis of the thermal behavior of wireless power transfer systems for electric vehicles. This is achieved by employing the reduced-order modeling approach considering radiation heat transfer. The analyses are performed using finite element analysis modeling software ANSYS workbench. We show that the accuracy of the system-level simulations utilizing the reduced-order model is sufficient compared to the results obtained from the corresponding magnetic-thermal coupled-field simulations. Moreover, experimental validations are carried out to determine the agreement of the reduced-order model with the test platform.

Index Terms—**Radiation heat transfer, magneto-thermal numerical simulations, thermal analysis, wireless power transfer.**

I. Introduction

THE analysis of wireless power transfer (WPT) systems through computational simulations is constantly a challenging task. This is due to the high complexity and resolution of the resulting numerical model and the needed computational power to solve it. Depending on the desired accuracy, the computational effort is considerable and hence the solution time is very long, leading to delays and limitations in associated design processes. The use of reduced-order modeling techniques to solve the mathematical equations of large-scale models is widely acknowledged as a mean to tackle the computational complexity, resulting in a substantial decrease in the solution time [1]. Moreover, it is essential to understand the thermal behavior and the extent of the temperature-rise of the WPT components. First, because of safety reasons (e.g., thermal runaway), second, because temperature rise negatively affects the system's efficiency [2]. Hence, based on that understanding, proper measures such as cooling or passive thermal systems using heat shields are needed to guarantee the operational safety and reliability of the WPT system [3]. Most of the studies addressing the thermal behavior of the WPT system do not analyze radiation heat transfer [2], [4]–[6]. The authors in [5] mention the amounts of radiative heat dissipation of a WPT system. Yet, no detailed modeling or analysis of its effects on the thermal behavior of the system is provided. Our previous work in [2] focused on the magneto-thermal coupled-field dynamic simulations of a WPT system and analyzing the operation frequency effect on its thermal characteristic. The WPT system was considered thermally decoupled, which means the reduced-order model did not consider the radiation between the surfaces of the ground assembly (GA) and the vehicle assembly (VA) modules. However, including the radiation heat transfer in the reduced model is necessary to correctly describe the thermal behavior and therefore extract a reduced-order model (ROM) that best matches the physical system. The model-order reduction approach is applied to the thermal field problem and the resulting behavioral ROMs are incorporated into the system-level simulations.

II. Proposed Approach

Thermal radiation in wireless power transfer applications usually involves only heat fluxes through the surfaces since the model materials do not allow internal radiation at the temperatures the system is expected to reach [8]. In that case, thermal radiation breaks up into radiation to ambient and surface-to-surface radiation, see (Fig. 1a). Our approach approximates the emitted radiations from the system surfaces and integrates them as effective thermal resistances in the system-level simulations. Extending the behavioral reduced-order model of the WPT system with approximated-radiation thermal resistances creates more accurate results.

In thermal radiation, the heat exchange depends on three factors: the size of the surfaces through which the energy exchange occurs, the separation distance between those surfaces, and the orientation angle of each surface to the other. These factors are accounted for by a geometric view factor function F. In the case of a stationary wireless power transfer, two surfaces are mainly involved in thermal radiation consideration. In the case of our experimental setup, these are the surfaces of the GA and VA acrylic plates. Accordingly, two view factors are required, F_{1-2} and F_{2-1}. The view factor (F_{1-2}) defines the fraction of the field-of-view of the GA side surface occupied by the VA side surface. In the same way, the view factor (F_{2-1}) defines the fraction of the field-of-view of the VA side surface occupied by the GA side surface. Generally, for different surfaces in size, shape, or orientation, the view factors are not equal and can be calculated using the equations in [9, p. 556],

$$\mathrm{F}_{1-2} = \frac{1}{A_1} \int_{A_1} \int_{A_2} \frac{\cos\beta_1 \cos\beta_2}{\pi s^2} dA_1 dA_2, \tag{1}$$

$$\mathrm{F}_{2-1} = \frac{1}{A_2} \int_{A_2} \int_{A_1} \frac{\cos\beta_2 \cos\beta_1}{\pi s^2} dA_2 dA_1, \tag{2}$$

where, s is the distance between the surfaces, β_1 and β_2 are the angles between the surface normals, and a ray between the two differential areas dA_1 and dA_2 of the surfaces s_1 and

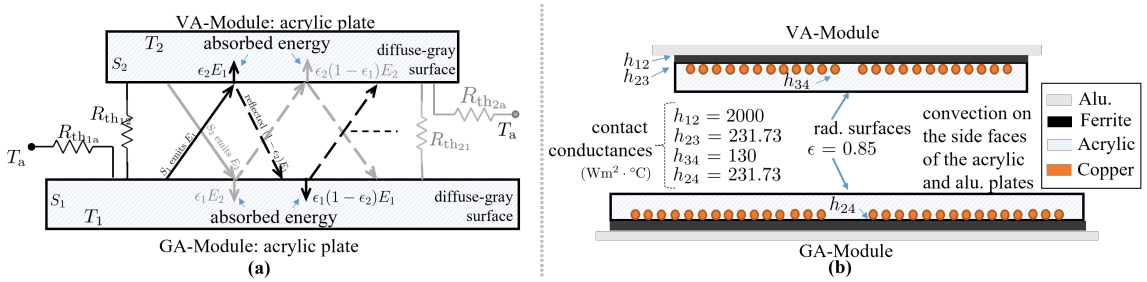

Fig. 1. (a) Radiative heat transfer between the surfaces of the acrylic plates of the GA and VA modules, based on the discussion in [7]. (b) shows an illustration of the GA and VA modules representative of the experimental setup considered in this work. The different thermal boundaries and contact conductances are given.

s_2, respectively. The direct calculation of these equations is cumbersome. For our considered model configuration, we use the evaluation expressions given in [10, p. 605]. It suffices to calculate one view factor and use the view factor reciprocity theorem, $A_1\mathrm{F}_{1-2} = A_2\mathrm{F}_{2-1}$, to calculate the other one. The heat transfer at an interface is generally described by $\dot{Q} = hA\Delta T$, where, h ($\mathrm{W}\cdot\mathrm{m}^{-2}$) is the heat transfer coefficient. ΔT (K) is temperature difference. For the wireless charging system under consideration, the equation of heat transfer through the acrylic plates involves both convection and radiation $\dot{Q} = \dot{Q}_\mathrm{c} + \dot{Q}_\mathrm{r} = h_\mathrm{total} A\Delta T$. The convective heat transfer coefficient is determined as discussed in our earlier work [2], the radiation heat tranfer coefficient is determined as follows. The rate of radiative heat transfer of a body with absolute temperature T_b, is governed by the Stephan-Boltzman equation: $\dot{Q}_\mathrm{r} = \epsilon\sigma A T_\mathrm{b}^4$, where, the parameter ϵ is the emmisivity of the surface of the body, which is constant for diffuse-gray surfaces, the parameter σ $=5.67\times10^{-18}\,\mathrm{W/m^2K^4}$ is the Stephan-Boltzman constant, and the parameter A is the surface area (m^2) of the body surface of radiation. The net rate of radiated heat flow of a body with temperature T_b in a surrounding with an average temperature T_a is:

$$\dot{Q}_{\mathrm{r\ net}} = \epsilon\sigma A(T_\mathrm{a}^4 - T_\mathrm{b}^4). \tag{3}$$

In wireless power transfer, to describe the net rate of heat transfer by radiation between the upper and downward surfaces of the GA and VA acrylic plates, respectively, (3) is updated to consider the view factors F of the surfaces:

$$\dot{Q}_{\mathrm{r\ net}} = \mathrm{F}\sigma\epsilon A(T^4 - T_\mathrm{b}^4) + (1-\mathrm{F})\sigma\epsilon A(T^4 - T_\mathrm{a}^4). \tag{4}$$

Looking at the differential form of Fourier's law of thermal conduction, considering that the thickness of the acrylic plates is constant, then the thermal resistance $R(\mathrm{K}\cdot\mathrm{W})$ is given as,

$$R = \Delta T/\dot{Q} = 1/(hA). \tag{5}$$

To build the extended reduced-order model in the system-level simulations, the thermal resistances for coupling the GA and VA modules need to be defined. From (4) and (5) the thermal resistances between two radiating surfaces R_ths and between each surface and the surrounding R_tha can be defined as follows:

$$R_{\mathrm{ths}_{12}} = 1/\mathrm{F}_{1-2}\sigma\epsilon(T_1+T_2)(T_1^2+T_2^2)A, \tag{6}$$
$$R_{\mathrm{tha}_1} = 1/(1-\mathrm{F}_{1-2})\sigma\epsilon(T_1+T_\mathrm{a})(T_1^2+T_\mathrm{a}^2)A, \tag{7}$$
$$R_{\mathrm{tha}_2} = 1/(1-\mathrm{F}_{2-1})\sigma\epsilon(T_2+T_\mathrm{a})(T_2^2+T_\mathrm{a}^2)A. \tag{8}$$

where the temperatures T_a, T_1, and T_2 correspond to the temperatures shown in Fig. 1a. Comparing equations (6)-(8) with (5), the radiation heat transfer coefficient is determined.

III. The Simulation Model

Fig. 2 depicts the model of the WPT system considered in this work. This arrangement resembles the model used in the experimental setup shown later in Section V. The calculated view factors by (1) and (2) for this arrangement are: F_{1-2} = 0.1628, and F_{2-1} = 0.8372. The coils are embedded in carrying acrylic plates, illustrated in Fig. 1b, are not shown in this figure for clarity. The lumped parameters of this model are $[L_\mathrm{p}, L_\mathrm{s}, M] = [169.7, 53, 32]$ µH, $[R_\mathrm{p}, R_\mathrm{s}] = [76, 23]$ mΩ

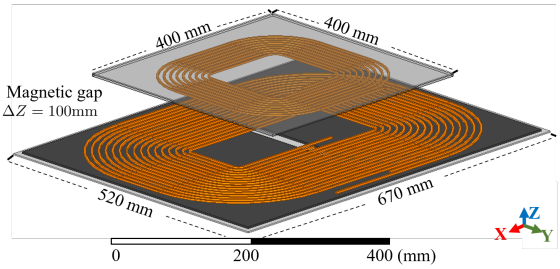

Fig. 2. Arrangement illustration of the GA and VA modules representative of the experimental setup.

The boundary conditions and the thermal contact conductances for the transient thermal simulations are shown in Fig. 1b. The defined thermal contact conductance coefficient between the coils and both the acrylic plates and the ferrite bars is based on the calculations in our previous work [2]. The contact conductance coefficient between the ferrite and the aluminum plates is set to $2000\,\mathrm{Wm^{-2}\cdot K^{-1}}$, and between the acrylic plate and the aluminum plate is set to $130\,\mathrm{Wm^{-2}\cdot K^{-1}}$.

For the order reduction of the WPT model, we used MORACT [11] *(Model Order Reduction Application Customization Toolkit)*, which implements the second-order Arnoldi reduction (SOAR) algorithm in ANSYS. Each WPT module is reduced separately, with the dimensions of each reduced model being n =20, this concerns reducing the thermal problem only. The result of the reduction is two behavioral models that are included in the system-level simulations. For that, we used Twin Builder from ANSYS Electronics Desktop.

At this point, the WPT modules are thermally-decoupled. In the system-level simulation, the resulting reduced-order models are extended and connected through the thermal resistances approximating the radiation heat transfer described by (6)-(8). This approach has many advantages: the solution time in the system-level simulations using the ROM models is in seconds which is a substantial speedup compared to the 3D magneto-thermal coupled-field simulation time, which might take several hours to converge. The complexity of the resulting models is manageable, so no specialized simulation clusters are required. Furthermore, the applied loads of the system can be defined or imported flexibly and without much loss of time. However, before the reduced models are used in subsequent simulation steps, it is essential to identify the accuracy of the reduced models separately, as addressed in the next section.

IV. Accuracy of the Reduced-Order Model

For determining the reduction error, the GA and VA modules are order-reduced and analyzed separately in transient thermal analyses. The power loss of the coils is considered homogeneous. A convection film coefficient of $5\ \mathrm{W/(m^2 \cdot °C)}$ is applied to the surfaces of the aluminum and acrylic plates of each module (see Fig. 1b for more details on the applied thermal boundary conditions). Figure 3 shows the average temperatures of the coil and the aluminum plate of both the GA and VA modules in the system-level and the 3D magneto-thermal coupled-field simulations. The co-simulation between the magnetic and thermal fields in ANSYS Workbench serves as a reference model. The applied joule heating for each coil is $50\,\mathrm{W}$. The reduction error, in this case, is 1.6% and 0.6% for the VA and GA modules, respectively. This discrepancy is considered acceptable for our application.

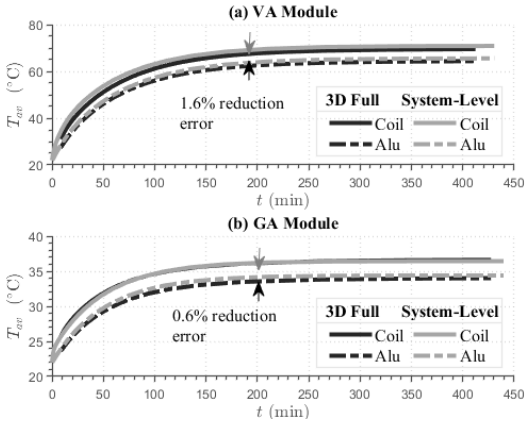

Fig. 3. The results of the system-level simulations of the reduced-order model of the GA and VA modules compared to the results of the corresponding 3D coupled-field simulations in ANSYS Mechanical.

The next step is determining the reduction error of the complete WPT system, which means the GA and VA modules are thermally coupled both in the system-level and transient thermal simulations, as the workflow illustrated in Fig.4 shows. Using the MORACT tool and APDL *(ANSYS Parametric Design Language)*, it is possible to export the eddy and ohmic losses calculated in the magnetic field solver to be used as inputs to the modules ROMs in the system-level simulation.

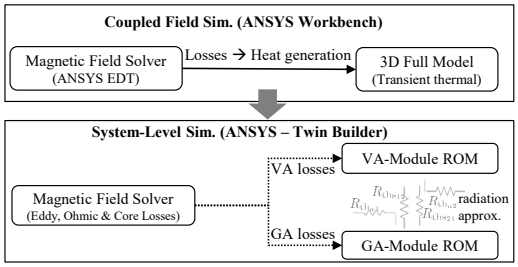

Fig. 4. Workflow of the ROM verification procedure.

Table I lists the average temperatures of the different WPT components and the accuracy of the reduced-order model (ROM). The values in Table I correspond to a transferred output power of $5\,\mathrm{kW}$ with 98% efficiency. Comprehensive magento-thermal field analyses of the WPT system, as explained in the previous work [2], serve as a verification of the reduced-order model and are listed in the second column of the table.

TABLE I
Accuracy of the WPT-ROM

	Average temp. °C	Coupled-field sim.	System-level sim.	Reduction error [%]
GA	$T_{\mathrm{avg,Coil}}$	60.6	66	8.9
	$T_{\mathrm{avg,Alu.}}$	62.5	63.4	6.7
VA	$T_{\mathrm{avg,Coil}}$	45.4	53.2	17
	$T_{\mathrm{avg,Alu.}}$	45	53.4	18.6

V. Experimental Setup and Results

The WPT system of the experimental setup consists of GA and VA modules, with GA and VA coils that are designed following the design specifications of the Test Stand GA WPT2 and Test Stand VA WPT2/Z2, respectively, given in the SAE standard J2954 [12]. The coils are made of AWG41 Litz wires made of 1575 single wires. The total conductor cross-section is $6.2357\,\mathrm{mm^2}$. Each coil is embedded in an acrylic plate fixture. The ferrite bars are fixed directly on the aluminum plate. Serial-serial compensation is used and built with type MLCC *(Multilayer ceramic capacitors)* capacitors. For the thermal measurements, three thermometers of type PCE-T390 are used, with four temperature sensors each.

TABLE II
The electrical parameters of the experiment.

Vin [V]	Iin [A]	Vout [V]	Iout [A]	Rl [Ω]
250	20.7	238	19.7	12

The measured total power dissipation is $500\,\mathrm{W}$. The power dissipation of the inductive coupler is measured to be $300\,\mathrm{W}$. The measurements are done using the power analyzer Hioki PW6001. The results of the ROM simulations agree with the records of the experiment for the VA module, as shown in Fig. 6. The discrepancy between simulation and experiment results for the GA module is around 14% at worst for the

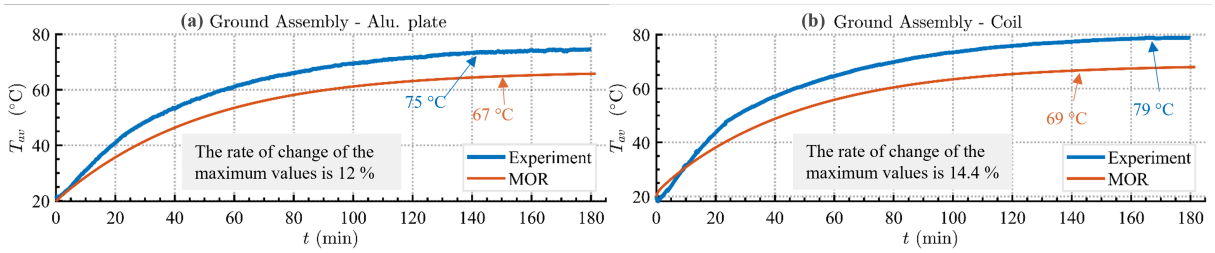

Fig. 5. The results of the ROM system-level simulations versus the records of the experiment for the (a) aluminum plate, and the (b) coil of the GA module.

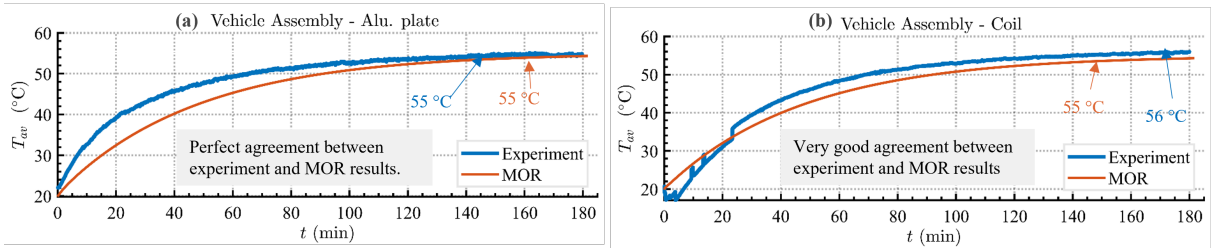

Fig. 6. The results of the ROM system-level simulations versus the records of the experiment for the (a) aluminum plate, and the (b) coil of the VA module.

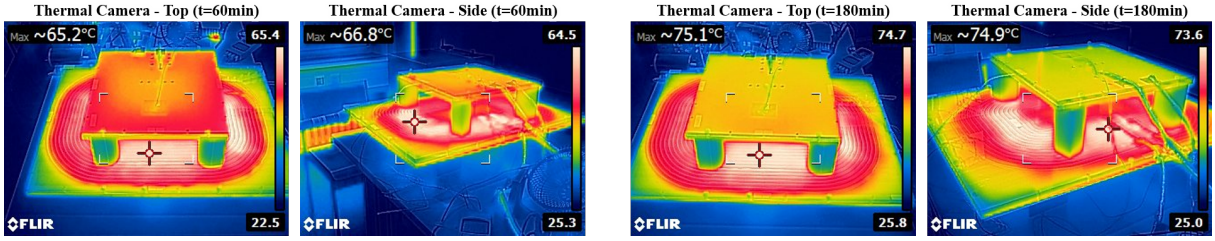

Fig. 7. Top and side view thermal camera images of the experiment, left-hand side at t=60 min and t=180 min at the right-hand side.

coil. This is an improvement of 44% compared to our work in [2] where radiation was not considered. The corresponding infrared images of the thermal camera are shown in Fig. 7.

VI. Conclusion

Our approach develops a validated basis for a realistic evaluation of the thermal characteristics of wireless charging systems. Validating the use of reduced-order modeling renders the examinations of the thermal behavior of wireless power transfer systems under varying influencing parameters and conditions such as different power levels and misalignment feasible. That is key to conceiving measures ensuring the efficiency and safety of those systems.

Acknowledgment

This work was funded by the Federal Ministry for Economic Affairs and Climate Action (BMWK), grant number 01MV21020A.

References

[1] P. Benner, S. Gugercin, and K. Willcox., "A Survey of Projection-Based Model Reduction Methods for Parametric Dynamical Systems," *SIAM Review 57*, pp. 483–531, Jun. 2015.

[2] M. Alsayegh, M. Saifo, M. Clemens, and B. Schmuelling, "Magnetic and Thermal Coupled Field Analysis of Wireless Charging Systems for Electric Vehicles," *IEEE Transactions on Magnetics*, Vol. 55.6, pp. 1–4. 2019.

[3] H. Zhao, Y. Wang, H. H. Eldeeb, J. Ge, J. Kang and O. A. Mohammed, "Determining the Optimal Range of Coupling Coefficient to Suppress Decline in WPTS Efficiency Due to Increased Resistance With Temperature Rise," *IEEE Open Journal of the Industrial Electronics Society*, vol. 1, pp. 148-156, 2020.

[4] S. Zimmer, M. Helwig, P. Lucas, A. Winkler,N. Modler, "Investigation of Thermal Effects in Different Lightweight Constructions for Vehicular Wireless Power Transfer Modules," *World Electric Vehicle Journal*, vol. 11, Oct 2020, 10.3390/wevj11040067.

[5] C. Zhu et al., "Thermal Simulation and Optimization Study for Magnetic Coupler of Static Electric Vehicle Wireless Power Transfer Systems," *22nd International Conference on Electrical Machines and Systems (ICEMS)*, pp. 1-4, 2019.

[6] C. Liang et al., "Modeling and Analysis of Thermal Characteristics of Magnetic Coupler for Wireless Electric Vehicle Charging System," *IEEE Access*, vol. 8, pp. 173177–173185, Jan. 2020.

[7] Z. S. Spakovszky, "Unified: Thermodynamics and Propulsion:19.3 Radiation Heat Transfer Between Planar Surfaces," Available at https://web.mit.edu/16.unified/www/SPRING/thermodynamics/notes/node136.html, Accessed Jun. 10, 2021.

[8] M. F. Modest, "Radiated Heat Transfer," *3rd. Elsevier Inc.*, 2013. ISBN: 978-0-12-386944-9.

[9] J. H. Lienhard IV, and J. H. Lienhard V, "A Heat Transfer Textbook," *5th. Mineola, NY: Dover Publications*, pp. 554–560, Dec.2019.

[10] W. M. Rohsenow, J. P. Hartnett, and Y. I. Cho, "Handbook of Heat Transfer," *3rd. McGraw-Hill Education*, 1998. Chap. 7., pp. 1520.

[11] CADFEM, "Model Reduction Inside ANSYS," 2020, "https://www.cadfem.net/en/our-solutions/cadfem-ansys-extensions/model-reduction-inside-ansys.html, Lastchecked = "27.08.2021".

[12] SAE J2954, "Wireless Power Transfer for Light Duty Plugin Electric Vehicles and Alignment Methodology," "https://www.sae.org/standards/content/j2954 201711/, Lastchecked = "27.08.2021".